Journal of Microscopy

*Journal of Microscopy*, Vol. 257, Issue 1 2015, pp. 54–64
*Received 16 June 2014; accepted 20 August 2014*

doi: 10.1111/jmi.12185

# Harmonic demodulation and minimum enhancement factors in field-enhanced near-field optical microscopy

A.F. SCARPETTINI*,‡ & A.V. BRAGAS*,†

*Laboratorio de Electrónica Cuántica, Departamento de Física, Facultad de Ciencias Exactas y Naturales, Universidad de Buenos Aires (1428), Buenos Aires, Argentina

†IFIBA-CONICET-UBA (1428), Buenos Aires, Argentina

**Key words.** Enhancement factor, harmonic demodulation, scanning near-field optical microscopy.

## Summary

Field-enhanced scanning optical microscopy relies on the design and fabrication of plasmonic probes which had to provide optical and chemical contrast at the nanoscale. In order to do so, the scattering containing the near-field information recorded in a field-enhanced scanning optical microscopy experiment, has to surpass the background light, always present due to multiple interferences between the macroscopic probe and sample. In this work, we show that when the probe–sample distance is modulated with very low amplitude, the higher the harmonic demodulation is, the better the ratio between the near-field signal and the interferometric background results. The choice of working at a given $n$ harmonic is dictated by the experiment when the signal at the $n+1$ harmonic goes below the experimental noise. We demonstrate that the optical contrast comes from the $n$th derivative of the near-field scattering, amplified by the interferometric background. By modelling the far and near field we calculate the probe–sample approach curves, which fit very well the experimental ones. After taking a great amount of experimental data for different probes and samples, we conclude with a table of the minimum enhancement factors needed to have optical contrast with field-enhanced scanning optical microscopy.

## Introduction

Design of plasmonic nanostructures with remarkable optical antenna properties such as strong confinement and high-field enhancement became one of the central issues in optical near-field imaging with nanometre spatial resolution (Eghlidi *et al.*, 2009; Scarpettini *et al.*, 2009 Barcelo *et al.*, 2012; Umakoshi *et al.*, 2012; Balzarotti & Stefani, 2012, Johnson *et al.*, 2012; Höppener *et al.*, 2012; De Angelis *et al.*, 2010; Cherukulappurath *et al.*, 2013). Experimental efforts to obtain better, robust and repeatable plasmonic probes are necessarily complemented with calculations of the enhancement factors as a measure of the potential performance of a given new design (Esteban *et al.*, 2009; Perassi *et al.*, 2011; Esteban *et al.*, 2012; Alonso-González *et al.*, 2012; Maximiano *et al.* 2012). However, one question arises: how much field enhancement and confinement is needed for a given experimental situation? Is it always necessary a probe with the maximum possible enhancement to get nanometre resolution? It is obvious that the answer depends a lot on multiple factors such as the materials involved, the experimental setup, background noise and desired resolution, among others. In this paper we analyse the scattered optical signal in typical near-field imaging and we end up with a table of minimum enhancement factors, based on simple fully analytical calculations and data collected in experimental real situations.

In field-enhanced scanning optical microscopy (FESOM) a laser beam illuminates the probe–sample junction exciting surface plasmons, strongly enhancing the electric field and confining it in a region whose size is on the order of the characteristic length of the probe. This probe acts as an intense source of light, locally exciting the sample and inducing a spectroscopic response. The scattered light from the near field, that contains information of the local optical properties of the sample, is detected in the far field together with a background coming from scattering centres in the probe and sample. The performance depends strongly on the polarization of the light, on the material, shape, size and structure of the probe and on the sample material.

In the usual FESOM configuration, the probe–sample distance is modulated at a frequency $\Omega$, so that the elastic backscattering is collected in a photodiode and the optical information is recovered using lock-in detection at a given harmonic of the modulation frequency. This higher harmonic

‡Present address: Laboratorio de Optoelectrónica y Metrología Aplicada, Facultad Regional Delta, Universidad Tecnológica Nacional, 2804 Campana, Argentina.
Correspondence to: Alberto Scarpettini, Laboratorio de Optoelectrónica y Metrología Aplicada, Facultad Regional Delta, Universidad Tecnológica Nacional, 2804 Campana, Argentina. Tel: 0054 3489 420400; e-mail: ascarpettini@frd.utn.edu.ar

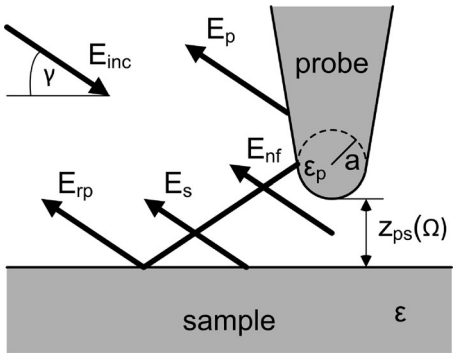


**Fig. 1.** The gap between the probe and the sample is irradiated by the incoming light $E_{\text{inc}}$, and the collected backscattered light is composed by the electric fields $E_p$ (scattered by the probe), $E_s$ (scattered by the sample), $E_{rp}$ (the probe reflected in the sample) and $E_{\text{nf}}$ (the near-field propagating component).

demodulation improves the ratio between the near-field signal and the interferometric background, due to the much higher nonlinearity of the near field as a function of the probe–sample distance (Labardi *et al.*, 2000; Maghelli *et al.*, 2001; Hillenbrand *et al.*, 2001; Walford *et al.*, 2001; Hillenbrand & Keilmann, 2002; Kim *et al.*, 2005). But if one wants optical contrast in FESOM, the near-field signal must surpass the scattered background (Chuang & Lo, 2007; Cvitkovic *et al.*, 2007; Behr & Raschke, 2008; Esteban *et al.*, 2009; Liao & Lo, 2011).

In this work we provide an extensive analysis of the harmonic demodulation and its relationship with the minimum enhancement factor needed to obtain the desired spatial resolution. We introduce an empiric roughness parameter to estimate the optical background, through a great number of experimental values collected with some probes and samples. They will allow us to estimate the minimum field enhancement factors needed to have optical contrast in high-resolution (elastic and Raman) imaging.

## Near-field detection

The backscattered light coming from the probe–sample junction is collected and collimated by an objective and sent to a photodiode. The photodiode output signal $V_p$ will be proportional to the incoming light intensity, which in turn will be proportional to the square modulus of the sum of the electric field $E_{\text{nf}}$ coming from the probe–sample zone and the scattered electric fields $E_p$, $E_s$ and $E_{rp}$ from the rest of the probe, the sample and the reflected probe by the sample, respectively. $E_{\text{nf}}$ is the far-field term that corresponds to the near electric field generated in the interaction region between the probe and the sample (see Fig. 1). Experimentally we observe that the field scattered by the sample is much lower than by the probe, so we can neglect $E_s$. Then we can write:

$$V_p \propto (E_{\text{nf}} + E_p + E_{rp})(E_{\text{nf}} + E_p + E_{rp})^*. \tag{1}$$

These fields interfere with each other causing amplifications and artefacts. If the plasmonic probe provides enough confinement and enhancement so that $E_{\text{nf}}$ surpass the background scattering produced by $E_p$ and $E_{rp}$, then we will have an optical signal with local chemical information of the sample.

If we have an incident radiation with wave vector $\mathbf{k}_i$ that is scattered with wave vector $\mathbf{k}_o$ by an object located in $\mathbf{r}$, there will be a change of phase $(\mathbf{k}_o - \mathbf{k}_i) \cdot \mathbf{r} = \Delta\mathbf{k} \cdot \mathbf{r}$. Then the scattered fields can be written as

$$E_p = |E_p| e^{i(\Delta\mathbf{k}\cdot\mathbf{r}_p - \omega t + \varphi_{ps})}, \tag{2}$$

$$E_{rp} = |E_{rp}| e^{i(\Delta\mathbf{k}\cdot(2\mathbf{r}_s - \mathbf{r}_p) - \omega t + \varphi_{ps})}, \tag{3}$$

where $\mathbf{r}_p$ is the probe position, $\mathbf{r}_s$ is the sample position under the probe, and $\varphi_{ps}$ is an arbitrary phase.

Given a probe and a sample of a determined material and shape, both illuminated by radiation with known polarization, then we can assume that the amplitude of the field $E_{\text{nf}}$ will only depend on the probe–sample distance. Then we can express the field $E_{\text{nf}}$ as

$$E_{\text{nf}} = |E_{\text{nf}}(|\mathbf{r}_s - \mathbf{r}_p|)| e^{i(\Delta\mathbf{k}\cdot\mathbf{r}_s - \omega t + \varphi_{ps})}. \tag{4}$$

As the sample is vibrating in $z$ at a frequency $\Omega$ with a very low amplitude $\delta z$, and considering that the $(x, y)$ scanning frequencies are much lower than $\Omega$, the sample position is given by

$$\mathbf{r}_s(x, y, z) \approx \mathbf{r}_{s0}(x, y) + \delta z \cos(2\pi\Omega t + \varphi)\hat{z}, \tag{5}$$

where $\varphi$ is an arbitrary phase. Defining $h(x, y) = |\mathbf{r}_{s0} - \mathbf{r}_p|$ then

$$\Delta\mathbf{k} \cdot (\mathbf{r}_{s0} - \mathbf{r}_p) = \Delta\mathbf{k} \cdot (-h\hat{z}) = -\Delta k_z h. \tag{6}$$

If we also define the instantaneous probe–sample distance

$$z_{ps} = h - \delta z \cos(2\pi\Omega t + \varphi), \tag{7}$$

then the expression (1) becomes

$$\begin{aligned} V_p \propto\ & |E_{\text{nf}}(z_{ps})|^2 + |E_p|^2 + |E_{rp}|^2 \\ & + 2|E_{\text{nf}}(z_{ps})||E_p| \cos(-\Delta k_z z_{ps}) \\ & + 2|E_{\text{nf}}(z_{ps})||E_{rp}| \cos(-\Delta k_z z_{ps}) \\ & + 2|E_p||E_{rp}| \cos(-2\Delta k_z z_{ps}). \end{aligned} \tag{8}$$

The incident field on the sample and its reflection are related by the Fresnel equations through the reflection coefficient $R$. So, the reflected scattered field by the probe is $|E_{rp}| = R|E_p|$. In the same way, if $|E_{p(ns)}|$ is the scattered field by the probe with no sample (with the probe totally retrieved, far from the sample), then $|E_p| = (1 + R)|E_{p(ns)}|$ because the probe is irradiated directly and by the reflection in the sample. Moreover, as experimentally the scattering from the probe is greater than the scattering from the sample due to the shape and roughness of the probe and the flatness of the sample, we define a parameter $\eta$ that contains these contributions, and we will

call it *roughness parameter* ($\eta \geq 1$). This parameter depends on the shape, material and roughness of the probe, its illuminated fraction, so it can be different from probe to probe. So, we can assume that $|E_{p(ns)}| = \eta |E_s|$. Then, we can rewrite (8) as

$$V_p \propto |E_{\mathrm{nf}}(z_{ps})|^2 + 2(1+R)^2\eta |E_{\mathrm{nf}}(z_{ps})||E_s|\cos(-\Delta k_z z_{ps}) + (1+R)^2\eta^2|E_s|^2[1+R^2+2R\cos(-2\Delta k_z z_{ps})]. \quad (9)$$

*Harmonic demodulation*

As $\delta z << h$, we can expand the field $E_{\mathrm{nf}}$ around $h$, and we can also expand the cosines around $\Delta k_z h$. Expanding again the powers of the cosines in higher harmonics of the argument, and if we hold only the lower order terms in $\delta z$, we can obtain approximate expressions of the optical signal coming from the scattering of light in the probe–sample junction for each harmonic component of the modulation frequency $\Omega$. For the continuous background, i.e. the term without modulation, we obtain

$$V_0 \propto E_{\mathrm{nf}}^2(h) + 2(1+R)^2\eta E_{\mathrm{nf}}(h)|E_s|\cos(\Delta k_z h) + (1+R)^2\eta^2|E_s|^2[1+R^2+2R\cos(2\Delta k_z h)] + o(\delta z^2). \quad (10)$$

The first term on the right corresponds to the near-field signal, the following term is an amplification of the same signal because it is multiplied by the background, and the remaining terms correspond to the background coming from all the other scattering centres in the probe and sample. The output voltages of the lock-in in the first three harmonics of the modulation frequency are

$$V_\Omega \propto \big[ - E_{\mathrm{nf}}(h)E'_{\mathrm{nf}}(h) + 2(1+R)^2\eta|E_s|[E_{\mathrm{nf}}(h)\sin(\Delta k_z h)\Delta k_z - E'_{\mathrm{nf}}(h)\cos(\Delta k_z h)] + 4R(1+R)^2\eta^2|E_s|^2 \times \sin(2\Delta k_z h)\Delta k_z\big]\delta z + o(\delta z^3), \quad (11)$$

$$V_{2\Omega} \propto \big[\frac{1}{4}E_{\mathrm{nf}}(h)E''_{\mathrm{nf}}(h) + \frac{1}{2}E'^2_{\mathrm{nf}}(h) + \frac{1}{2}(1+R)^2\eta|E_s|\big[-E_{\mathrm{nf}}(h)\cos(\Delta k_z h)\Delta k_z^2 - 2E'_{\mathrm{nf}}(h)\sin(\Delta k_z h)\Delta k_z + E''_{\mathrm{nf}}(h)\cos(\Delta k_z h)\big] - 2R(1+R)^2\eta^2|E_s|^2\cos(2\Delta k_z h)\Delta k_z^2\big]\delta z^2 + o(\delta z^4), \quad (12)$$

$$V_{3\Omega} \propto \big[-\frac{1}{24}E_{\mathrm{nf}}(h)E'''_{\mathrm{nf}}(h) - \frac{1}{8}E'_{\mathrm{nf}}(h)E''_{\mathrm{nf}}(h) + \frac{1}{12}(1+R)^2\eta|E_s|\big[-E_{\mathrm{nf}}(h)\sin(\Delta k_z h)\Delta k_z^3 + 3E'_{\mathrm{nf}}(h)\cos(\Delta k_z h)\Delta k_z^2 + 3E''_{\mathrm{nf}}(h)\sin(\Delta k_z h)\Delta k_z - E'''_{\mathrm{nf}}(h)\cos(\Delta k_z h)\big] - \frac{2}{3}R(1+R)^2\eta^2|E_s|^2\sin(2\Delta k_z h)\Delta k_z^3\big]\delta z^3 + o(\delta z^5), \quad (13)$$

where $E'_{\mathrm{nf}}$, $E''_{\mathrm{nf}}$ and $E'''_{\mathrm{nf}}$ are the first, second and third derivatives of $E_{\mathrm{nf}}$ respect $z$.

We could calculate an arbitrary harmonic $n$ of the signal, but it weakens as $n$ increases, and in practice, as we can see later, it will be enough these first three terms. The structure of all these signals is similar: we have terms with products of near-field derivatives, several crossed terms between the near field and the background and the interferometric signal of the background corresponding to each harmonic.

*Background analysis*

As in our experiment we collect the backscattering, the change in the wave vector on the Eq. (6) is given by $\Delta\mathbf{k} = 2\mathbf{k}_o$, whose $z$ component is

$$\Delta k_z = 2k_o \sin\gamma = \frac{4\pi}{\lambda}\sin\gamma, \quad (14)$$

being $\gamma$ the incident and collection angle. The spatial period $\Gamma_z$ in $z$ of the interferometric signal arises from the sines and cosines in the background terms in expressions (11–13). Then, it is $2\Delta k_z \Gamma_z = 2\pi$ and, together with the expression (14), we obtain that

$$\Gamma_z = \frac{\lambda}{8\sin\gamma}. \quad (15)$$

We added a factor 1/2 in the spatial frequency because the lock-in gives back positive values in the output voltage, i.e. the modulus of the cosine. Moreover, a similar argument allows us to obtain the spatial period $\Gamma_{xy}$ of the interferometric signal on the plane of the sample. The wave number variation on the plane is

$$\Delta k_{xy} = 2k_o \cos\gamma = \frac{4\pi}{\lambda}\cos\gamma, \quad (16)$$

and setting again the condition $\Delta k_{xy}\Gamma_{xy} = 2\pi$, and assuming that the interference is mounted on the near-field signal, we obtain

$$\Gamma_{xy} = \frac{\lambda}{2\cos\gamma}. \quad (17)$$

We can also obtain the maximum amplitude of the background signal in the $n$th harmonic ($B_{n\Omega}$) from expressions (11) to (13), and we show in Figure 2 its dependence with the incident angle $\gamma$, suggesting that there is an optimal irradiation and collection angle for each probe–sample pair. Comparing the maximum amplitude of the background signal in a particular harmonic with the corresponding in the following harmonic, we observe that

$$\frac{B_{2\Omega}}{B_\Omega} = \frac{\Delta k_z \delta z}{2}, \qquad \frac{B_{3\Omega}}{B_{2\Omega}} = \frac{\Delta k_z \delta z}{3}. \quad (18)$$

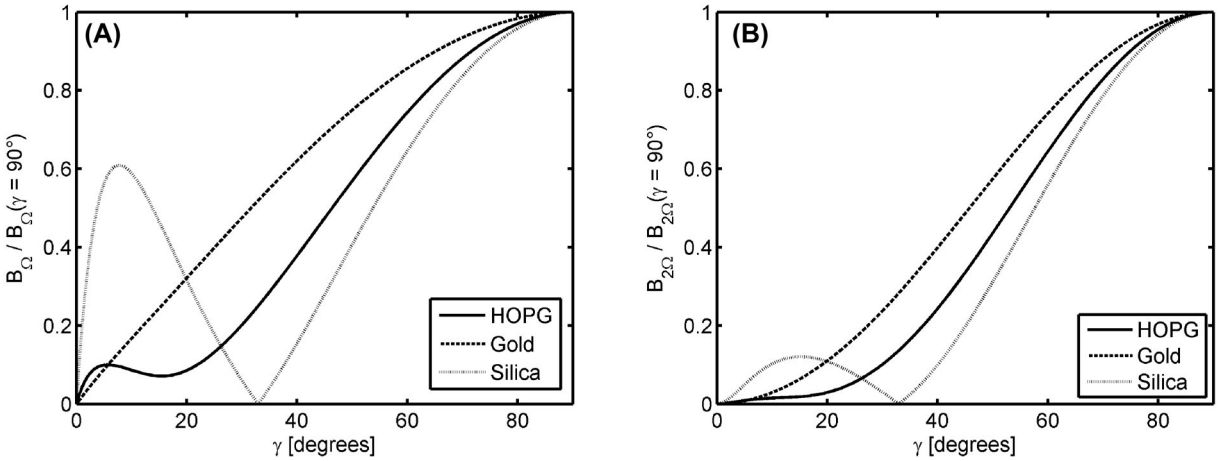


**Fig. 2.** Maximum amplitude of the background signal in the (A) first and (B) second harmonic compared to the normal incidence case, as function of the incident angle for HOPG, gold and silica samples.

As $\Delta k_z \delta z << 1$, *the interferometric signal amplitude fall down quickly as we move to higher harmonics of the modulation frequency*. As we will see, with this higher harmonic demodulation the near-field signal can overcome the background from a certain harmonic onwards.

From expression (10) we obtain the maximum amplitude of the continuous background $B_0 = (1+R)^4 \eta^2 |E_s|^2$, so we can derive the roughness parameter

$$\eta = \frac{\sqrt{B_0}}{(1+R)^2 |E_s|}. \tag{19}$$

We estimated this parameter empirically, to include it on the calculations. For this, we did statistics on the detected optical signal in the approach curves for each kind of probe and sample. We obtained values of $\eta$ in the order of a few tens.

Generally the crossed terms in Eqs (11)–(13) exceed the ones that contain only near-field scattering, unless the enhancement factors are very high. We can roughly estimate the relation between the field $E_{\mathrm{nf}}$ and the fields coming from the scattering centres in the probe ($E_p$) and the sample ($E_s$). The field $E_{\mathrm{nf}}$ come from a confined and enhanced zone in the probe–sample junction, whose area is on the order of $a^2$, being $a$ the characteristic length of the probe and the confinement. On the other hand, all the scattering centres in the probe and the sample fill an area in the order of $\omega_0^2$, being $\omega_0$ the half waist of the focused beam. This means that, if there are no enhancement, the ratio between the scattered intensities from each area is on the order of $a^2/\omega_0^2$. So, the ratio between the scattered fields scales as $a/\omega_0$.

Being $f$ the near-field enhancement factor, and considering the expression (11), the ratio between the near-field term and the crossed term that contains the first derivative of the optical signal at $\Omega$ is

$$\left| \frac{E_{\mathrm{nf}} E'_{\mathrm{nf}} \delta z}{2(1+R)^2 \eta |E_s| E'_{\mathrm{nf}} \cos(\Delta k_z h) \delta z} \right| \sim \left| \frac{E_{\mathrm{nf}}}{(1+R)^2 \eta |E_s|} \right| \sim \frac{fa}{(1+R)^2 \eta \omega_0}. \tag{20}$$

Both terms will be on the same order, i.e. the expression (20) approaches 1, if the enhancement factor is on the order of $(1+R)^2 \eta \omega_0 / a$. As in general $a$ is much lower than $\eta\omega_0$, it will be necessary a great enhancement to take into account the term that contains only the near field and its derivatives. It is the same with the detected signal in higher harmonics of $\Omega$. For this reason, *the main terms are the crossed products between the near field and the background*, that provide a genuine amplification of the information coming from the point of the sample that it is sensed by the FESOM.

### *Near-field dependence to the distance*

Now we want to know how the near-field (and its derivatives) dependence is with the probe–sample distance, to estimate the detected optical signals in each harmonic, described in expressions (11–13). The simple model that consist of a unique effective dipole in front of a plane surface is very useful because it predicts enhancements and scattering cross sections for long working distances, on the order of the characteristic length of the nanostructure and greater, very similar to that obtained with the more complex and detailed simulations using Generalized Multiparticle Mie theory (Fuller & Kattawar, 1988; Xu & Gustafson, 2001) or Discrete Dipole Approximation (Purcell & Pennypacker, 1973; Draine & Lee, 1984). But it fails when the working distances are very small, in the near contact region. In these situations, the more complex numeric models predict enhancements and scattering cross sections higher than in the case of a centred dipole in the nanostructure (Ruppin, 1983; Porto *et al.*, 2003; Keilmann & Hillenbrand, 2004). Moreover, the enhancement grows considerably if conic macroscopic tips are studied, because they can reach higher charge concentrations

(Martin *et al.*, 2001; Krug *et al.*, 2002; Novotny & Stranick, 2006; Esteban *et al.*, 2007).

We can use a dipolar model of the interaction between the probe and the sample to predict optical properties in far field and near field (Knoll & Keilmann, 2000; Keilmann & Hillenbrand, 2004). This is the simplest model but we use it to explicitly demonstrate the above relationships. Any model that depends more strongly with the distance will be better. The part of the probe nearest to the sample, which is responsible of the optical interaction, can be approximated by a polarizable sphere of radius $a$, much smaller than the wavelength of the incident radiation. Being $\varepsilon_p$ the complex dielectric constant of the probe material, its polarizability $\alpha$ is given by

$$\alpha = 4\pi a^3 \frac{\varepsilon_p - 1}{\varepsilon_p + 2}. \tag{21}$$

In the electrostatic limit, when $a << \lambda$ (Bohren & Huffman, 1998), the effective polarizability of the probe–sample dipolar system (for $p$- and $s$-polarization) is

$$\alpha_{\text{eff}}^{(p)} = \frac{\alpha(1+\beta)}{1 - \frac{\alpha\beta}{16\pi z^3}}, \qquad \alpha_{\text{eff}}^{(s)} = \frac{\alpha(1-\beta)}{1 - \frac{\alpha\beta}{32\pi z^3}}, \tag{22}$$

where $z = a + h$, with $h$ the probe–sample distance, and

$$\beta = \frac{\varepsilon - 1}{\varepsilon + 1}. \tag{23}$$

being $\varepsilon$ the complex dielectric constant of the sample. The intensity and direction of the dipolar response of the probe–sample (sphere–plane) system will depend on the polarization of the incident field. The enhancement factor $f$ is defined by

$$f^{(p)} = \frac{|\alpha_{\text{eff}}^{(p)}|}{|\alpha|} = \frac{|1+\beta|}{\left|1 - \frac{\alpha\beta}{16\pi z^3}\right|},$$

$$f^{(s)} = \frac{|\alpha_{\text{eff}}^{(s)}|}{|\alpha|} = \frac{|1-\beta|}{\left|1 - \frac{\alpha\beta}{32\pi z^3}\right|}. \tag{24}$$

The radiated field $E_{\text{nf}}$ by the probe–sample dipolar system that reaches the detector is proportional to the incident field (Bohren & Huffman, 1998), that is

$$E_{\text{nf}} \propto k^2 \alpha_{\text{eff}} E_{\text{inc}}, \tag{25}$$

and the scattering cross section is

$$C_{\text{sca}} = \frac{k^4}{6\pi} |\alpha_{\text{eff}}|^2. \tag{26}$$

It is important to notice that the effective polarizability $\alpha_{\text{eff}}$ provides the necessary contrast to chemically sense the sample. During the scanning of the probe over the sample, all the parameters of the probe remain constant, and the variations in the detected optical signal are exclusively due to changes in the dielectric constant of the sample or in the probe–sample distance. This dipolar model predicts a red shift of the plasmon when the probe is very close to the sample, reaching enhancements lower than one order of magnitude. If we compare these results with our experiments (Scarpettini *et al.*, 2009) or with other works using Generalized Multiparticle Mie or Discrete Dipole Approximation (Porto *et al.*, 2003; Romero, 2006; García de Abajo, 2008; Encina & Coronado, 2010; Perassi *et al.*, 2011), the reached enhancements and red shifts are lower. This configuration clearly do not model the optical properties at small probe–sample distances, but it do at long distances. The problem is that this model does not take into account the electromagnetic interactions between the surface of the probe and the sample when they are extremely close, because the probe dipole and the image dipole are located in the centre of the spheres, at a distance of one diameter. This model neither takes into account the multipolar terms (Ruppin, 1983). However, we will continue with the centred dipole model to underestimate the optical properties and to show that the reached enhancements are enough to obtain contrast in images.

We must first calculate the derivatives of the field $E_{\text{nf}}$ to estimate the approach curves in each harmonic of the modulation frequency and to know if the enhanced near field can surpass the background scattering. If we choose an incident radiation with $p$ polarization, and according to Eq. (25), the field scattered by the enhanced zone in the probe–sample junction is proportional to the effective polarizability $\alpha_{\text{eff}}$, and is given by

$$E_{\text{nf}} = \frac{ck^2\alpha(1+\beta)}{1 - \frac{\alpha\beta}{16\pi z^3}}, \tag{27}$$

where $c$ is a proportionality constant. The derivative respect $z$ of this field is

$$E'_{\text{nf}} = \frac{3E_{\text{nf}}}{z\left(1 - \frac{16\pi z^3}{\alpha\beta}\right)}. \tag{28}$$

If we continue deriving we obtain

$$E''_{\text{nf}} = \frac{2E'_{\text{nf}}\left(1 + \frac{32\pi z^3}{\alpha\beta}\right)}{z\left(1 - \frac{16\pi z^3}{\alpha\beta}\right)} = \frac{6E_{\text{nf}}\left(1 + \frac{32\pi z^3}{\alpha\beta}\right)}{z^2\left(1 - \frac{16\pi z^3}{\alpha\beta}\right)^2}. \tag{29}$$

These relations allow us to compare the crossed terms of the near field with the background in expressions (11) and (12) of the optical signal detected at $\Omega$ and $2\Omega$, respectively. In the first case, if we consider short probe–sample distances, the ratio between the crossed term with the no derived field and the term that contain the first derivative is

$$\left|\frac{2(1+R)^2\eta|E_s|E_{\text{nf}}\sin(\Delta k_z h)\Delta k_z \delta z}{2(1+R)^2\eta|E_s|E'_{\text{nf}}\cos(\Delta k_z h)\delta z}\right| \sim \left|\frac{E_{\text{nf}}\Delta k_z}{E'_{\text{nf}}}\right| = \frac{z\Delta k_z}{3}\left(1 - \frac{16\pi z^3}{\alpha\beta}\right) << 1, \tag{30}$$

because we showed that $\Delta k_z$ goes as the wavelength and so $z\Delta k_z << 1$, and also $\alpha$ goes as $a^3$. This means that, in the signal detected at $\Omega$, the largest term that compete against

background is the term that contains the first derivative of the near field multiplied (amplified) by the same background. In the following case, the signal detected at 2Ω, the ratio between the crossed term with the first derivative and the term with the second derivative is

$$\left|\frac{(1+R)^2\eta|E_s|E'_{\mathrm{nf}}\sin(\Delta k_z h)\Delta k_z \delta z^2}{1/2(1+R)^2\eta|E_s|E''_{\mathrm{nf}}\cos(\Delta k_z h)\delta z^2}\right| \sim \left|\frac{2E'_{\mathrm{nf}}\Delta k_z}{E''_{\mathrm{nf}}}\right| = z\Delta k_z \frac{1-\frac{16\pi z^3}{\alpha\beta}}{1+\frac{32\pi z^3}{\alpha\beta}} << 1. \quad (31)$$

Again, this means that in the signal detected at 2Ω, the largest crossed term in the competence against background is the term that contains the second derivative of the near field. Following so on, *in the optical signal detected at n harmonic, the local chemical information is mainly given by the nth-derivative respect to z of the enhanced field confined in the zone between probe and sample*.

*Approach curves*

At this point, we can estimate the approach curves for each wavelength. We used tables of references (Johnson & Christy, 1972; Palik, 1985) to obtain the complex dielectric constant of several materials as function of frequency. In Figure 3(A) we show an approach curve at Ω calculated from expression (11), in the case of 633 nm irradiation, using a silver sphere of 10 nm radius approaching a HOPG substrate. We consider an average case that is a probe with roughness $\eta = 15$. We can observe the characteristic interferometric pattern in the form of the modulus of cosine due to background scattering, with spatial periods that depend on the incidence angle and the wavelength, as expressed in Eq. (15). The phase of the interferometric pattern was arbitrary chosen.

Calculated from expression (12), in Figure 3(B) we can see an approach curve at 2Ω for the same case. In the same figure, we can see an inset with a detailed near contact zone. The background scattering gone down several orders of magnitude but we can still observe the characteristic interferometric pattern at long distances. However, the signal coming from the near field largely exceeds the background from a few nanometres to contact. This signal variation is sharp in the last nanometres, indicating that it is a good candidate to obtain high vertical resolution when imaging at short working distances. If the sample has a better plasmonic response than the graphite, this sensibility would be higher.

In our FESOM the laser beam is focused in a 5 $\mu$m diameter region. The sample vibrates at a few kHz frequency, with an amplitude range of 0.01–0.3 nm. In Figures 3(C,D) we show experimental approach curves obtained with the FESOM using a silver nanoparticle-based probe on a HOPG sample (Scarpettini *et al.*, 2009). They were irradiated with a 633 nm laser line and the detection was performed at Ω and 2Ω. It can be clearly seen the correspondence between these curves and the numeric results in Figures 3(A,B).

*Minimum enhancement factors*

We can estimate the minimum enhancement factor $f_1$ such that the near-field signal can equals the background signal for a given probe–sample distance and a given wavelength, if we calculate the ratio between the highest crossed term and the background term in expression (11) which corresponds to the optical signal detected at the modulation frequency Ω. This ratio is

$$\left|\frac{2(1+R)^2\eta|E_s|E'_{\mathrm{nf}}\cos(\Delta k_z h)\delta z}{4R(1+R)^2\eta^2|E_s|^2\sin(2\Delta k_z h)\Delta k_z \delta z}\right| \sim \left|\frac{E'_{\mathrm{nf}}}{2R\eta|E_s|\Delta k_z}\right| \sim \left|\frac{3E_{\mathrm{nf}}}{2R\eta|E_s|z\Delta k_z\left(1-\frac{16\pi z^3}{\alpha\beta}\right)}\right| \sim \frac{3f_1 a}{2R\eta\omega_0 z\Delta k_z\left|1-\frac{16\pi z^3}{\alpha\beta}\right|}. \quad (32)$$

If we want that these two terms are similar, i.e. the ratio equals 1, then the minimum enhancement factor is

$$f_1 = \frac{2R\eta\omega_0}{3a} z\Delta k_z \left|1-\frac{16\pi z^3}{\alpha\beta}\right|. \quad (33)$$

This minimum enhancement factor can be seen in Figure 4(A), for the same previous case. These extremely high enhancement values are necessary because the background is very intense at the modulation frequency Ω. However, at near contact distances this factor goes down to reasonable values. A good probe may obtain contrast using detection at the fundamental modulation frequency if it can efficiently confine and enhance the electric field. But the background signal will still be very intense.

As in the previous case, the minimum enhancement factor $f_2$ such that the near-field signal in approach curve at 2Ω may equals the background signal for a given probe–sample distance and a given wavelength can be obtained calculating the ratio between the highest crossed term (that contains the second derivative) and the background term in expression (12), that is

$$\left|\frac{1/2(1+R)^2\eta|E_s|E''_{\mathrm{nf}}\cos(\Delta k_z h)\delta z^2}{2R(1+R)^2\eta^2|E_s|^2\cos(2\Delta k_z h)\Delta k_z^2\delta z^2}\right| \sim \left|\frac{E''_{\mathrm{nf}}}{4R\eta|E_s|\Delta k_z^2}\right| \sim \left|\frac{3E_{\mathrm{nf}}\left(1+\frac{32\pi z^3}{\alpha\beta}\right)}{2R\eta|E_s|z^2\Delta k_z^2\left(1-\frac{16\pi z^3}{\alpha\beta}\right)^2}\right| \sim \frac{3f_2 a}{2R\eta\omega_0 z^2\Delta k_z^2}\frac{|1+\frac{32\pi z^3}{\alpha\beta}|}{|1-\frac{16\pi z^3}{\alpha\beta}|}. \quad (34)$$

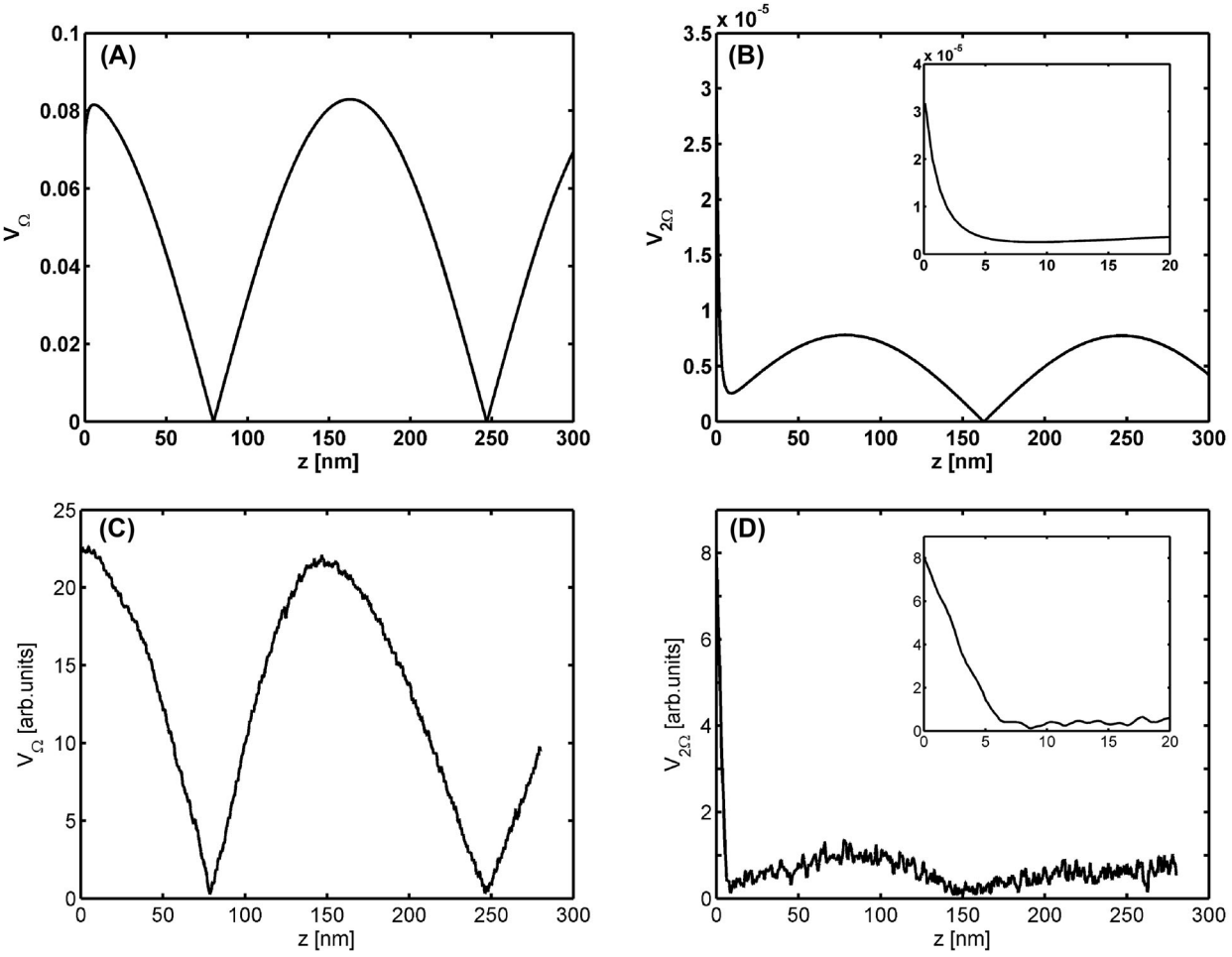


**Fig. 3.** (A, B) Approach curves of a silver sphere of 10 nm radius on a HOPG sample, detecting at frequencies (A) Ω and (B) 2 Ω, irradiated with 633 nm light. The inset in (B) shows the curve in the near contact zone. (C, D) Experimental approach curves of a silver nanoparticle-based probe on a HOPG sample irradiated with 633 nm light, detecting at (C) Ω and (D) 2 Ω.

If we want that these two terms are comparable (equal), we obtain an expression for the enhancement factor, given by

$$f_2 = \frac{2R\eta\omega_0}{3a} z^2 \Delta k_z^2 \frac{\left|1 - \frac{16\pi z^3}{\alpha\beta}\right|}{\left|1 + \frac{32\pi z^3}{\alpha\beta}\right|}. \tag{35}$$

This factor $f_2$ can be seen in Figure 4(B). We can observe that the minimum enhancement factor $f_2$ needed to overcome the background scattering in detection at 2Ω is much lower than in the Ω detection case. Indeed, from Eqs (33) and (35) we have

$$\frac{f_2}{f_1} = \frac{z\Delta k_z}{\left|1 + \frac{32\pi z^3}{\alpha\beta}\right|} << 1. \tag{36}$$

In this case the minimum enhancements are relatively low for short distances, being promissory the detection in the second harmonic because the background went down considerably. We can repeat this analysis for the subsequent harmonics of the optical signal, and we will see that the ratio between the near-field scattering and the background will improve as we demodulate in higher harmonics. The problem is that the optical signal will become weaker, being undetectable above certain harmonic. There is a compromise between these two aspects and we must choose the optimal working harmonic. To do so we use approach curves, which allow us to get images knowing completely the optical response of the probe.

These minimum enhancement factors needed to get a near-field signal over the background scattering in each detecting harmonic were calculated for a spherical probe. So high symmetrical probe is the worst candidate to reach high-field intensities, but even so they allow optical resolution if we work in higher harmonics. A nonspherical shaped probe, with some end point or protuberance, will get more confinement of the electric field and higher enhancements (Kelly *et al.*, 2003; Encina *et al.*, 2009; Perassi *et al.*, 2010). A macroscopic but

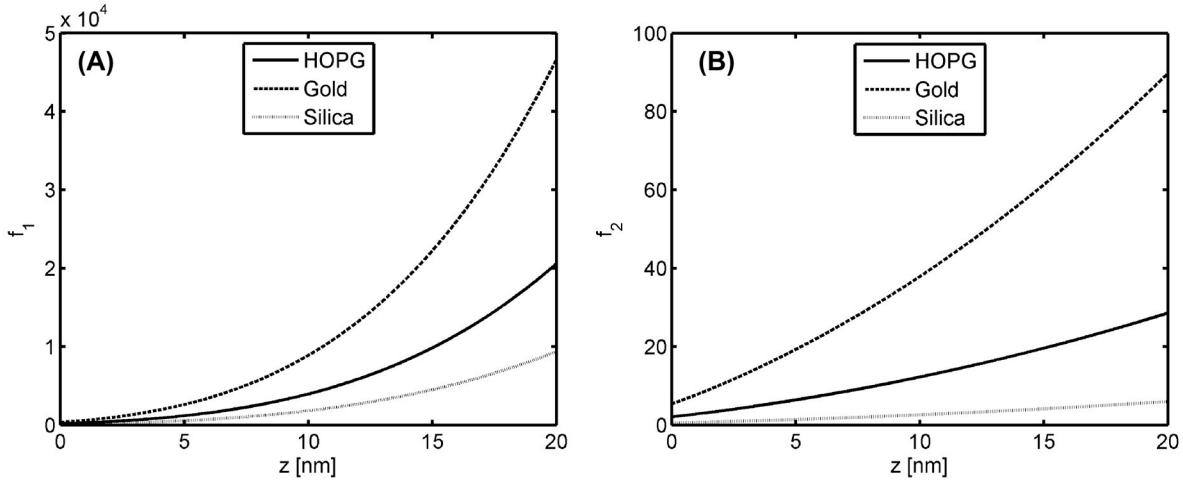


**Fig. 4.** Minimum enhancement factors needed to equals the near-field scattering to the background, as function of the probe–sample distance, detecting at frequencies (A) Ω and (B) 2 Ω, and irradiated with 633 nm wavelength, for a 10 nm silver sphere on HOPG, gold and silica samples.

sharp probe will get higher field enhancements compared to a nanosphere whose radius is equal to the curvature radius of the tip apex (Esteban *et al.*, 2007). In the last case is extremely difficult the repeatability in the tip fabrication, i.e. to obtain two tips that confine and enhance the field in the same way. It is easy to obtain very sharp tips by etching processes, but with poor control on the final shape and apex size. The use of metal nanoparticles has the advantage that we can build nanostructures with more control on involved dimensions, and so on the field confinement (Kalkbrenner *et al.*, 2001; Anger *et al.*, 2006; Vakarelski & Higashitani, 2006; Höppener & Novotny, 2008; Scarpettini *et al.*, 2009; Eghlidi *et al.*, 2009; Perassi *et al.*, 2011).

On the other way, if we know the structure, material and dimensions of the probe, we can estimate the field confinement of the incident light around the probe. This means that if we want to study a sample with a given dielectric constant, it is very useful to know the minimum enhancement factor needed to chemically sense it. This factor will depend on the confinement reached by the probe and the optimal working wavelength. So, we built Table 1 with the minimum enhancements for some possible configurations, irradiating with 532 nm and 633 nm laser lines. In this example, we have a silver probe, illuminated with an angle of 28° and a focus waist of 5 $\mu$m, and a lock-in detection at the second harmonic of the backscattering. The table shows minimum enhancement factors given by Eq. (35) for different characteristic lengths of the probe and different samples. We assumed that the working distance is similar to the characteristic length of the probe. If we work closer, we will need lower enhancements, if we work further, we will need higher ones. In this estimation we include experimental measurements of the roughness parameter done with our FESOM over several probes and samples.

The table shows minimum enhancement factors lower than 400, and in some cases with very low values. The silica is the better sample to obtain optical contrast, requiring enhancements below 30, so it is a good sample to test a probe performance. The other samples require little higher factors, specially sputtered gold that, despite its good plasmonic response, it has high reflectivity generating so much background scattering. If we demodulate in a higher harmonic, these minimum enhancement factors will become lower.

These minimum factors to overcome the background given by Eq. (35) are model dependent. In this case, the dipolar model centred in the sphere give us the higher possible values. A model that takes into account the electromagnetic interactions between the probe and sample surfaces when they are very close will need lower enhancement factors. It will be the same if we consider the interaction in dimers or in higher order aggregates of spheres, or metallic tips whose apex has a similar size than the sphere. In all these cases it will be easier to surpass the background scattering. Then, the exposed table represents the worst scenario, but it gives us an idea of the field confinement and enhancement that must provide a probe to ensure optical contrast on each kind of sample.

### *Raman imaging*

In this operation mode, the probe scans the sample whereas both are illuminated from the far field. The collected backscattering is sent to a Raman spectrometer and the desired inelastic scattering is detected by a cooled charge-coupled device. For each position of the probe over the sample, i.e. for each pixel of the image, the charge-coupled device acquires a range of frequencies during a prefixed integration time. So, the probe–sample distance is not modulated and then the enhanced

**Table 1.** This table shows minimum enhancement factors for a silver probe on different samples, confinement radii and working distances, irradiated with light of 532 nm (green, $\lambda_g$) and 633 nm (red, $\lambda_r$), in the case of 2 Ω detection.

| Sample | $a = 2.5$ nm | | $a = 5$ nm | | $a = 10$ nm | | $a = 20$ nm | | a = 50nm | | a = 80nm | |
|---|---|---|---|---|---|---|---|---|---|---|---|---|
| | $\lambda_g$ | $\lambda_r$ | $\lambda_g$ | $\lambda_r$ | $\lambda_g$ | $\lambda_r$ | $\lambda_g$ | $\lambda_r$ | $\lambda_g$ | $\lambda_r$ | $\lambda_g$ | $\lambda_r$ |
| Silica | 1 | 1 | 2 | 1 | 4 | 3 | 7 | 5 | 18 | 13 | 29 | 21 |
| Gold | 11 | 9 | 23 | 19 | 45 | 38 | 91 | 76 | 227 | 190 | 364 | 304 |
| HOPG | 4 | 3 | 8 | 6 | 16 | 12 | 33 | 25 | 82 | 61 | 131 | 98 |
| Silicon | 5 | 3 | 10 | 6 | 19 | 13 | 39 | 25 | 96 | 63 | 154 | 100 |

Raman signal must surpass the inelastic scattering background at the same frequencies. The advantage in this case is that Raman scattering intensity scales to the fourth power of the enhancement factor of the electric field. In fact,

$$\frac{I_{\mathrm{nf}}}{I_s} = \frac{f^4 a^2}{\eta^2 \omega_0^2}, \tag{37}$$

being $I_{\mathrm{nf}}$ the intensity of the inelastic scattering from the probe–sample junction, where the field is confined in a region of radius $a$ and enhanced by a factor $f$, and $I_s$ is the intensity of the inelastic scattering by the rest of the sample, with roughness parameter $\eta$, illuminated by a laser beam with half waist $\omega_0$. In this way, we would have contrast if both intensities are, at least, of the same order. So, we can estimate the minimum enhancement factor $f_R$ needed to overcome the inelastic scattering background, which is

$$f_R = \sqrt{\frac{\eta \omega_0}{a}}. \tag{38}$$

For example, using our setup parameters and the roughness and field confinement values proposed in Table 1, the minimum enhancement factor $f_R$ varies from 22 to 122, which are reachable values in a FESOM experiment.

## Conclusions

If we modulate the probe–sample distance in a field-enhanced scanning optical microscope, the detected optical signal at a harmonic of the modulation frequency has three components: an unwanted background scattering, a component that contains only near-field scattering, and a near-field component amplified by the background. By increasing the harmonic demodulation, the near-field signal becomes more intense compared to the background. We show that detecting at $n$ harmonic, the near-field information basically come from its $nth$derivative respect the normal direction to the sample.

We used a well-known and simple dipolar model of the interaction between the probe and the sample and it proved to be sufficient to predict the optical response of the system in the far field and in the near field, without using sophisticated numerical methods. This model proposes minimum enhancements to reach, to chemically sense the sample, depending on its dielectric constant and probe roughness, on the wavelength and polarization of the incident radiation, and on the field confinement achieved with the probe. We predict approach curves at the first harmonics of the modulation frequency. We show a table with enhancement values to overcome, to obtain optical contrast on different kind of samples. These values correspond to spherical probes, and we expect that they will be lower if the spherical symmetry is broken, as in dimers, higher order aggregates or sharp-shaped probes. Finally, we show that moderate minimum enhancements are required to map the Raman scattering on the sample.

## References


Alonso-González, P., Albella, P., Schnell, M., *et al.* (2012) Resolving the electromagnetic mechanism of surface-enhanced light scattering at single hot spots. *Nat. Commun.* **3**, 684.

Anger, P., Bharadwaj, P. & Novotny, L. (2006) Enhancement and quenching of single-molecule fluorescence. *Phys. Rev. Lett.* **96**, 113002-1–113002-4.

Balzarotti, F. & Stefani, F.D. (2012) Plasmonics meets far-field optical nanoscopy. *ACS Nano.* **6**(6), 4580–4584.

Barcelo, S.J., Kim, A., Wu, W. & Li, Z. (2012) Fabrication of deterministic nanostructure assemblies with sub-nanometer spacing using a nanoimprinting transfer technique. *ACS Nano.* **6**(7), 6446–6452.

Behr, N. & Raschke, M.B. (2008) Optical antenna properties of scanning probe tips: plasmonic light scattering, tip-sample coupling, and near-field enhancement. *J. Phys. Chem. C* **112**, 3766–3773.

Bohren, C.F. & Huffman, D.R. (1998) *Absorption and Scattering of Light by Small Particles*. John Wiley & Sons, New York.

Bragas, A.V. & Martínez, O.E. (2000) Field-enhanced scanning optical microscope. *Opt. Lett.* **25**, 631–633.

Cherukulappurath, S., Johnson, T.W., Lindquist, N.C. & Oh, S.H. (2013) Template-stripped asymmetric metallic pyramids for tunable plasmonic nanofocusing. *Nano. Lett.* **13**, 5635–5641.

Chuang, C.H. & Lo, Y.L. (2007) Analytical analysis of modulated signal in apertureless scanning near-field optical microscopy. *Opt. Express* **15**(24), 15782–15796.

Cvitkovic, A., Ocelic, N. & Hillenbrand, R. (2007) Analytical model for quantitative prediction of material contrasts in scattering-type near-field optical microscopy. *Opt. Express* **15** (14), 8550–8565.

De Angelis, F., Das, G., Candeloro, P., *et al.* (2010) Nanoscale chemical mapping using three-dimensional adiabatic compression of surface plasmon polaritons. *Nat. Nanotech.* **5**, 67–72.

Draine, B.T. & Lee, H.M. (1984) Optical properties of interstellar graphite and silicate grains. *Astrophys. J.* **285**, 89–108.

Eghlidi, H., Lee, K.G., Chen, X.W., Götzinger, S. & Sandoghdar, V. (2009) Resolution and enhancement in nanoantenna-based fluorescence microscopy. *Nano. Lett.* **9**(12), 4007–4011.

Encina, E.R. & Coronado, E.A. (2010) Plasmon coupling in silver nanosphere pairs. *J. Phys. Chem. C* **114**, 3918–3923.

Encina, E.R., Perassi, E.M. & Coronado, E.A. (2009) Near-field enhancement of multipole plasmon resonances in Ag and Au nanowires. *J. Phys. Chem. A* **113**, 4489–4497.

Esteban, R., Borisov, A.G., Nordlander, P. & Aizpurua, J. (2012) Bridging quantum and classical plasmonics with a quantum-corrected model. *Nat. Commun.* **3**, 825.

Esteban, R., Vogelgesang, R. & Kern, K. (2007) Tip-substrate interaction in optical near-field microscopy. *Phys. Rev. B* **75**, 195410.

Esteban, R., Vogelgesang, R. & Kern, K. (2009) Full simulations of the apertureless scanning near field optical microscopy signal: achievable resolution and contrast. *Opt. Express* **17**(4), 2518–2529.

Fischer, U.C. & Pohl, D.W. (1989) Observation of single-particle plasmons by near-field optical microscopy. *Phys. Rev. Lett.* **62**, 458–461.

Fuller, K.A. & Kattawar, G.W. (1988) Consummate solution to the problem of classical electromagnetic scattering by an ensemble of spheres. *Opt. Lett.* **13**(2), 90–92.

García de Abajo, F.J. (2008) Nonlocal effects in the plasmons of strongly interacting nanoparticles, dimers, and waveguides. *J. Phys. Chem. C* **112**, 17983–17987.

Girard, C., Joachim, C. & Gauthier, S. (2000) The physics of the near-field. *Rep. Prog. Phys.* **63**, 893–938.

Hillenbrand, R. & Keilmann, F. (2002) Material-specific mapping of metal/semiconductor/dielectric nanosystems at 10 nm resolution by backscattering near-field optical microscopy. *Appl. Phys. Lett.* **80**, 25–27.

Hillenbrand, R., Knoll, B. & Keilmann, F. (2001) Pure optical contrast in scattering-type scanning near-field microscopy. *J. Microsc.* **202**, 77–83.

Höppener, C., Lapin, Z.J., Bharadwaj, P. & Novotny, L. (2012) Self-similar gold-nanoparticle antennas for a cascaded enhancement of the optical field. *Phys. Rev. Lett.* **109**, 017402-1–017402-4.

Höppener, C. & Novotny, L. (2008) Antenna-based optical imaging of single $Ca^{2+}$ transmembrane proteins in liquids. *Nano. Lett.* **8**(2), 642–646.

Inouye, Y. & Kawata, S. (1994) Near-field scanning optical microscope with a metallic probe tip. *Opt. Lett.* **19**(3), 159–161.

Johnson, P.B. & Christy, R.W. (1972) Optical constants of the noble metals. *Phys. Rev. B* **6**, 4370–4379.

Johnson, T.W., Lapin, Z.J., Beams, R., Lindquist, N.C., Rodrigo, S.G., Novotny, L. & Oh, S.H. (2012) Highly reproducible near-field optical imaging with sub-20-nm resolution based on template-stripped gold pyramids. *ACS Nano.* **6** (10), 9168–9174.

Kalkbrenner, T., Ramstein, M., Mlynek, J. & Sandoghdar, V. (2001) A single gold particle as a probe for apertureless scanning near-field optical microscopy. *J. Microsc.* **202**, 72–76.

Keilmann, F. & Hillenbrand, R. (2004) Near-field microscopy by elastic light scattering from a tip. *Phil. Trans. R. Soc. Lond. A* **362**, 787–805.

Kelly, K.L., Coronado, E., Zhao, L.L. & Schatz, G.C. (2003) The optical properties of metal nanoparticles: the influence of size, shape, and dielectric environment. *J. Phys. Chem. B* **107**, 668–677.

Kim, Z.H., Liu, B. & Leone, S.R. (2005) Nanometer-scale optical imaging of epitaxially grown GaN and InN islands using apertureless near-field microscopy. *J. Phys. Chem. B* **109**, 8503–8508.

Knoll, B. & Keilmann, F. (2000) Enhanced dielectric contrast in scattering-type scanning near-field optical microscopy. *Opt. Commun.* **182**, 321–328.

Krug II, J.T., Sánchez, E.J. & Sunney Xie X. (2002) Design of near-field optical probes with optimal field enhancement by finite difference time domain electromagnetic simulation. *J. Chem. Phys.* **116**(24), 10895–10901.

Labardi, M., Patanè, S. & Allegrini, M. (2000) Artifact-free near-field optical imaging by apertureless microscopy. *Appl. Phys. Lett.* **77**, 621–623.

Liao, C.C. & Lo, Y.L. (2011) Phenomenological model combining dipole-interaction signal and background effects for analyzing modulated detection in apertureless scanning near-field optical microscopy. *Prog. Electromagn. Res.* **112**, 415–440.

Maghelli, N., Labardi, M., Patanè, S., Irrera, F. & Allegrini, M. (2001) Optical near-field harmonic demodulation in apertureless microscopy. *J. Microsc.* **202**, 84–93.

Martin, Y.C., Hamann, H.F. & Wickramasinghe, H.K. (2001) Strength of the electric field in apertureless near-field optical microscopy. *J. Appl. Phys.* **89**(10), 5774–5778.

Maximiano, R.V., Beams, R., Novotny, L., Jorio, A. & Cançado, L.G. (2012) Mechanism of near-field Raman enhancement in two-dimensional systems. *Phys. Rev. B* **85**, 235434-1–235434-8.

Novotny, L. & Stranick, S.J. (2006) Near-field optical microscopy and spectroscopy with pointed probes. *Annu. Rev. Phys. Chem.* **57**, 303–331.

Palik, E.D. (1985). *Handbook of Optical Constants of Solids*. Academic Press, New York.

Perassi, E.M., Hernandez-Garrido, J.C., Moreno, M.S., Encina, E.R., Coronado, E.A. & Midgley, P.A. (2010). Using highly accurate 3D nanometrology to model the optical properties of highly irregular nanoparticles: a powerful tool for rational design of plasmonic devices. *Nano. Lett.* **10**(6), 2097–2104.

Perassi, E.M., Scarpettini, A.F., Masip, M.E., Bragas, A.V. & Coronado, E.A. (2011) Understanding the plasmonic properties of silica microspheres decorated with Ag nanoparticles as new probes for field enhanced scanning optical microscopy. *J. Phys. Chem. C* **115**, 10455–10461.

Porto, J.A., Johansson, P., Apell, S.P. & López-Ríos, T. (2003) Resonance shift effects in apertureless scanning near-field optical microscopy. *Phys. Rev. B* **67**, 085409-1–085409-9.

Purcell, E.M. & Pennypacker, C.R. (1973) Scattering and absorption of light by nonspherical dielectric grains. *Astrophys. J.* **186**, 705–714.

Romero, I., Aizpurua, J., Bryant, G.W. & García de Abajo, F.J. (2006) Plasmons in nearly touching metallic nanoparticles: singular response in the limit of touching dimers. *Opt. Express* **14**, 9988–9999.

Ruppin, R. (1983) Surface modes and optical absorption of a small sphere above a substrate. *Surf. Sci.* **127**, 108–118.

Sandoghdar, V. (2001) Trends and developments in scanning near-field optical microscopy. *Proceedings of the International School of Physics, "Enrico Fermi" course CXLIV* (ed. by M. Allegrini, N. García & O. Marti), pp. 65–119. IOS Press, Amsterdam.

Scarpettini, A.F., Pellegri, N. & Bragas, A.V. (2009) Optical imaging with subnanometric vertical resolution using nanoparticle-based plasmonic probes. *Opt. Commun.* **282**, 1032–1035.

Specht, M., Pedarnig, J.D., Heckl, W.M. & Hänsch, T.W. (1992) Scanning plasmon near-field microscope. *Phys. Rev. Lett.* **68**(4), 476–479.

Umakoshi, T., Yano, T., Saito, Y. & Verma, P. (2012) Fabrication of near-field plasmonic tip by photoreduction for strong enhancement

in tip-enhanced Raman spectroscopy. *Appl. Phys. Exp.* **5**, 052001-1–052001-3.

Vakarelski, I.U. & Higashitani, K. (2006) Single-nanoparticle-terminated tips for scanning probe microscopy. *Langmuir* **22**(7), 2931–2934.

Walford, J.N., Porto, J.A., Carminati, R., *et al.* (2001) Influence of tip modulation on image formation in scanning near-field optical microscopy. *J. Appl. Phys.* **89**(9), 5159–5169.

Wessel, J. (1985) Surface-enhanced optical microscopy. *J. Opt. Soc. Am. B* **2**(9), 1538–1541.

Xu, Y.I. & Gustafson, B.A.S. (2001) A generalized multiparticle Mie-solution: further experimental verification. *J. Quant. Spectrosc. Radiat. Transfer* **70**(4–6), 395–419.

Zenhausern, F., O'Boyle, M.P. & Wickramasinghe, H.K. (1994) Apertureless near-field optical microscope. *Appl. Phys. Lett.* **65**(13), 1623–1625.